Influence of oxygen in the production chain of Cu–Ti-based metallic glasses via laser powder bed fusion

Erika Soares Barreto, Jan Wegner, Maximilian Frey, Stefan Kleszczynski, Ralf Busch, Volker Uhlenwinkel, Lutz Mädler & Nils Ellendt

Published online: 16 Mar 2023.

Submit your article to this journal

Article views: 674

View related articles

View Crossmark data

I·M3
Institute of Materials,
Minerals & Mining

Taylor & Francis
Taylor & Francis Group

RESEARCH ARTICLE

OPEN ACCESS

Check for updates

Influence of oxygen in the production chain of Cu–Ti-based metallic glasses via laser powder bed fusion

Erika Soares Barreto [a,b], Jan Wegner[c], Maximilian Frey[d], Stefan Kleszczynski[c], Ralf Busch[d], Volker Uhlenwinkel[a,b], Lutz Mädler[a,b] and Nils Ellendt[a,b]

aLeibniz Institute for Materials Engineering – IWT, Bremen, Germany; bFaculty of Production Engineering, University of Bremen, Bremen, Germany; cChair of Manufacturing Technology, University of Duisburg-Essen, Duisburg, Germany; dChair of Metallic Materials, Saarland University, Saarbrücken, Germany

ABSTRACT

Laser powder bed fusion of metals (PBF-LB/M) is advantageous for manufacturing bulk metallic glasses with size and geometrical freedom. However, the oxygen uptake along the production chain can negatively impact the generation of high-quality, amorphous parts. In this context, Cu–Ti-based alloys were gas-atomised and additively manufactured using commercial- (CP) and high-purity (HP) feedstocks. The oxygen absorption in each processing step was tracked and related to the amorphous phase formation and glass-forming ability (GFA) of alloys. Results show an increasing oxygen absorption, considerably influenced by the starting feedstock, especially for CP. In HP material, the most contribution is inherent from the powder oxygen content. Results reveal the lack of influence of the oxygen content in the GFA. TEM analysis of commercial powder and PBF-LB/M sample show uniform and featureless micrographs, displaying the absence of oxygen-induced nucleation. The present contribution enhances the qualification and economic processability of amorphous metals by PBF-LB/M.

1. Introduction

Additive manufacturing (AM) is rapidly establishing as a production route for different material classes due to the process efficiency with size and geometrical freedom. Some AM techniques, particularly laser powder bed fusion of metals (PBF-LB/M), offer great potential in the synthesis of non-equilibrium microstructures because of the high cooling rates during the solidification of the melt pool [1–3]. Recently, PBF-LB/M is widely investigated to fabricate bulk metallic glasses (BMGs) as it can promote vitrification [4]. However, the glass-forming ability (GFA) of the feedstock powders is usually significantly lower than cast materials. Lower GFAs increase the likelihood of (nano)crystallisation during AM fabrication due to the complex thermal history inherent in the laser–material interaction with consecutive re-melting steps [1,2,4,5]. As subsequently processed layers experience additional heat, the already vitrified glassy parts may experience structural relaxation or crystallisation [6]. Consequently, especially the heat-affect zones (HAZ) in AM metallic glasses are more susceptible to devitrification [7]. The drawback is that the presence of crystallites could compromise the generation of high-quality, amorphous parts [2,4,5,8].

The presence of oxygen in glass-forming alloys can pose a significant challenge in the production and processing of superior bulk metallic glasses. The production chain of BMGs via PBF-LB/M is more susceptible to oxygen contamination than conventional casting [9,10]. One reason is the generally poorer atmosphere of processing chambers and repeated melting steps compared to casting. Owing to the oxygen entrapment and humidity in the powder feedstock, as well as the surface-to-volume ratio governing oxygen uptake during atomisation, higher oxygen pick-up occurs along the production chain [2,8,9,11–13]. Besides, the processing gas atmosphere and feedstock purity influence the vitrification process in metallic glasses [1,10,13,14]. Studies show that, if above a certain level, the presence of oxygen can reduce the GFA of BMGs and aid the nucleation and growth of crystals, so reducing the overall amorphous fraction [4,5,7,14–19]. Likewise, higher oxygen concentrations in additively manufactured BMGs are correlated to narrowed AM-processing windows and deteriorated mechanical strength caused either by the oxygen embrittlement of the amorphous matrix or the presence of nano-scaled crystallites. [2,4,5,8–10,13,20–22]. Thus, PBF-LB/M of BMGs is mostly performed with expensive high-purity (HP) materials

---

CONTACT Erika Soares Barreto ✉ sbarreto@iwt.uni-bremen.de 🏢 Leibniz Institute for Materials Engineering — IWT Materials, Badgasteiner Str. 3, 28359, Bremen, Germany; Faculty of Production Engineering, University of Bremen, Bremen, Germany

instead of commercial purity (CP, industrial-grade), constraining their broad commercialisation [11]. For instance, it was reported that crystallisation could not be avoided in an industrial-purity Zr-based alloy ($Zr_{59.3}Cu_{28.8}Al_{10.4}Nb_{1.5}$, in at.%, tradename AMZ4) manufactured with gas-atomised amorphous powders with an oxygen content around 1300 ppm [23]. In this context, tracking the oxygen uptake along the production chain and its influence on BMGs properties highly contributes to producing cost-efficient, high-strength amorphous metal components, especially when CP materials are selected as feedstocks.

The present work evaluates the oxygen absorption during powder production via gas atomisation and additive manufacturing of HP and CP Cu–Ti-based glass formers. The impact of oxygen contamination on the GFA and amorphous phase formation is evaluated. The compositions $Cu_{47}Ti_{34}Zr_{11}Ni_8$ (Vit101), $Cu_{47}Ti_{33}Zr_{11}Ni_8Si_1$ (Vit101Si) and $Cu_{47}Ti_{33}Zr_{11}Ni_6Sn_2Si_1$ (Vit101SiSn) were selected based on the highest GFA found for this system [24,25], besides the economic viability of starting elements.

2. Materials and methods

2.1 Powder production

Close-coupled gas atomisation (CCA) [11,26] was used to synthesise the Cu–Ti-based powders. Feedstock materials using single elements of different purities were directly mixed in high-purity, halogen-treated graphite crucibles (2120PT, Mersen) to obtain the targeted chemical composition. This benefits the process's cost-effectiveness by waiving the need for pre-casting into master alloys. The CP feedstock was comprised of CuNi (99.95 wt-%, in which 3.6 wt-% Ni), Ti (99.4 wt-%), Zr 702 (99.2 wt-%), Ni (99.8 wt-%), Si (99.99 wt-%) and Sn (99.98 wt-%), totalising 0.32 wt-% of impurities. To obtain the HP feedstock, the elements Cu (99.99 wt-%), Ti (99.4 wt-%), Zr crystal bar (99.97 wt-%) and Ni (99.9 wt-%) were used, computing for approx. 0.17 wt-% total impurities. A third purity degree was obtained from the HP feedstock by melting and solidifying the single elements directly inside the atomisation chamber, namely HP-remelted. The generated master alloy was sequentially re-melted and atomised. In the spray chamber, the

measured oxygen concentration was 100 ppm [11]. Table 1 summarises the experimental parameters of each gas-atomisation run. The gas pressure and nozzle diameter were increased for the atomisation runs of HP and HP-remelted feedstocks for respectively increasing the powder yield in the 20–63 μm fraction, as previously reported in [11], while maintaining a similar melt mass flow rate.

Powder classification in the desired 20–63 μm range for PBF-LB/M consisted of sieving below 250 μm to remove large splats, air-classification under nitrogen gas to remove fine particles (<20 μm), and subsequent sieving < 63 μm with a conventional sieving machine.

2.2 PBF-LB/M sample fabrication

Sample fabrication was carried out on a PBF-LB/M system (SLM 280 HL) equipped with two fibre lasers of 700 W with nominal laser spot sizes of approx. 70 μm. During the build process, the oxygen content was adjusted to an usual high concentration of 400–700 ppm to emphasize the oxygen uptake on samples for further evaluation. CP samples of Vit101, Vit101Si and Vit101SiSn, as well as HP and HP-remelted Vit101, were additively manufactured. Constant laser conditions were applied to build cylindrical specimens of dimensions (2.5×5 mm³, diameter × height) using preheated Ti substrates at 373 K (Table 2). The parameter selection was done based on previous work for a Zr-based metallic glass reported in [2].

2.3 Analyses

The oxygen content of samples was measured with hot gas carrier extraction (ELTRA ONH-2000) using helium (99.999%). The powder mass in each measurement weighted ca. 50 mg, whereas max. 300 mg was required for each PBF-LB/M sample and HP-remelted feedstock. In total, five measurements were conducted and the results were averaged. As humidity impacts powder flowability, drying is usually performed before PBF-LB/M manufacturing. Thus the influence of the drying atmosphere was investigated. The oxygen content in powder samples (20–63 μm) of Vit101 and

Table 1. Process conditions during gas atomisation used for powder synthesis.

Alloy	Purity	P (MPa)	T_{gas} (K)	Inert gas	D (mm)	ΔT_m (K)	$\dot{m}_G$ (kg h^{-1})	$\dot{m}_L$ (kg h^{-1})	GMR (–)	$d_{50,3}$ (μm)
Vit101	CP	1.2	293 (RT)	Argon	2	~500	592	149	4.0	52
Vit101Si								150	4.0	50
Vit101SiSn								150	3.9	47
Vit101	HP	1.6	293 (RT)	Argon	2.5	~500	780	152	5.1	44
Vit101	HP-remelted	1.6	293 (RT)	Argon	2.5	~500	780	146	5.3	38

Vit101 = $Cu_{47}Ti_{34}Zr_{11}Ni_8$, Vit101Si = $Cu_{47}Ti_{33}Zr_{11}Ni_8Si_1$, Vit101SiSn = $Cu_{47}Ti_{33}Zr_{11}Ni_6Sn_2Si_1$, CP = commercial purity, HP = high purity, HP-remelted = re-atomised HP feedstock, p = Atomisation gas pressure, T_{gas} = Initial gas temperature, RT = Atomisation gas at ambient temperature, D = Nozzle outlet diameter, ΔT_m = Superheated melt temperature, $\dot{m}_G$ = Gas mass flow rate, $\dot{m}_L$ = Melt mass flow rate, GMR = Gas-to-melt mass flow ratio, $d_{50,3}$ = Mass median particle diameter.

Table 2. PBF-LB/M fabrication parameters.

Laser power (P)	Scan speed (v)	Layer thickness (d)	Hatch distance (h)	Volume energy density (E_v)	Gas
60 W	1800 mm s^{-1}	20 μm	70 μm	23.8 J mm^3	Argon

Vit101Si dried under vacuum and argon was compared. Argon drying was carried out at room temperature for 72 h, whereas vacuum was performed at least five times for 30 min at 70°C. The differences in the drying procedures regard the oven specifications but are most likely comparable in reducing the moisture content.

Microsections of the manufactured samples were prepared from cross-sections along the build direction with hot embedding in epoxy resin for following grinding and polishing. The porosity analysis was performed using image analysis (PixelFerber) of optical micrographs (Stereomicroscope MZ16, Leica) of polished un-etched surfaces. The resulting percentage was calculated from the total pore area within each measurement field (4160×2320 μm). Energy-dispersive X-ray analysis (EDX) detector coupled to a scanning electron microscope (SEM, TESCAN VEGA II XLH) provided information of the chemical composition. Additionally, oxygen elemental mappings were measured for all PBF-LB/M samples with an electron microprobe (EMP, Jeol JXA8200) on an area of 300×300 μm. Each map was obtained with a 0.30-μm step size, 20 nA beam current, 15 kV accelerating voltage and 20 ms dwell time.

Differential scanning calorimetry (DSC, Perkin-Elmer DSC 8000) evaluated the thermal properties of Vit101 and Vit101Si powders of different class sizes containing distinct oxygen levels. Scans were performed under HP Argon flow (99.9999%) from 100°C to 580°C with 1 Ks^{-1} heating rate to obtain the glass transition onset temperatures T_g and the onset of crystallisation T_x.

Moreover, high-resolution transmission electron microscopy (HRTEM, FEI Titan 80/300) evaluated clusters formation and (nano-) crystallisation in the CP Vit101 powder and additively manufactured sample, which presented different oxygen levels and solidification routes. Focused ion beam scanning electron microscope (FIB-SEM, FEI Nova Nanolab 200) was used for lamella preparation by lift-out method followed by low kV thinning to generate an electron transparent region with max. 100 nm total thickness.

3. Results and discussion

The influence of argon and vacuum drying atmospheres on the oxygen uptake of CP Vit101 and Vit101Si powders (20–63 μm) was investigated before using the powder for PBF-LB/M. Argon drying led to a final oxygen concentration of 765 ± 29 ppm for Vit101 and 750 ± 12 ppm for Vit101Si. Similarly, a vacuum atmosphere resulted in 756 ± 12 ppm and 750 ± 9 ppm, respectively. The negligible differences suggest both methods equally suffice for avoiding additional oxygen pick-up. Subsequent additive manufacturing was carried out with powder dried under vacuum. Optical microscopy was performed to determine the porosity in the manufactured samples. Figure 1 displays representative micrographs of the cross-sections along the build direction. Relative densities above 99% were obtained for all Vit101 and Vit101Si samples. The highest density of 99.8% was measured for the CP Vit101, followed by HP Vit101 and Vit101Si with 99.6%, and 99.2% for the Vit101-remelted. With only 94.9% density, the largest defect formation was observed for Vit101SiSn, evidenced by the high porosity, lack of fusion, and horizontal cracks. This finding, while preliminary, suggests that the increased degree of microalloying compromised the PBF-LB/M processability. The fracture toughness of BMGs can exhibit significant variations even with minor composition alterations [27]. Previous research reported the toughness of as-cast Vit101 to reduce with Si and Sn additions [24]. As the alloy becomes more brittle, it most likely cannot withstand the intrinsic thermal cycles of the additive manufacturing process, justifying the higher defect formation and crack propagation. Because only one set of parameters was employed, a more detailed study would be required to enhance sample densification. It is expected that a lower porosity could be obtained with a more suitable processing window and better scanning strategies. For instance, increasing the heat input into the material, i.e. the volumetric energy density (E_v), is normally associated with better densification of AM specimens [10,28]. Nonetheless, the laser parameters should be carefully selected when processing BMGs, as higher E_v may also cause melt overheating which, in turn, reduces the cooling rate and facilitate crystallisation to occur [23,29,30]. Consequently, the synthesis of a fully amorphous bulk metallic glass should consider appropriate heating and cooling rates [22,31].

Prior research suggests that a threshold of 99.9% relative density should be accomplished for achieving satisfactory mechanical performance in bending tests [28]. The evaluation of mechanical properties is beyond the framework of this investigation and will be a topic of future studies.

EDS was performed to determine the compositions of the present phase. The data displayed in Figure 1(b) presents the corresponding peak spectra of the detected elements of Vit101. The elements identified
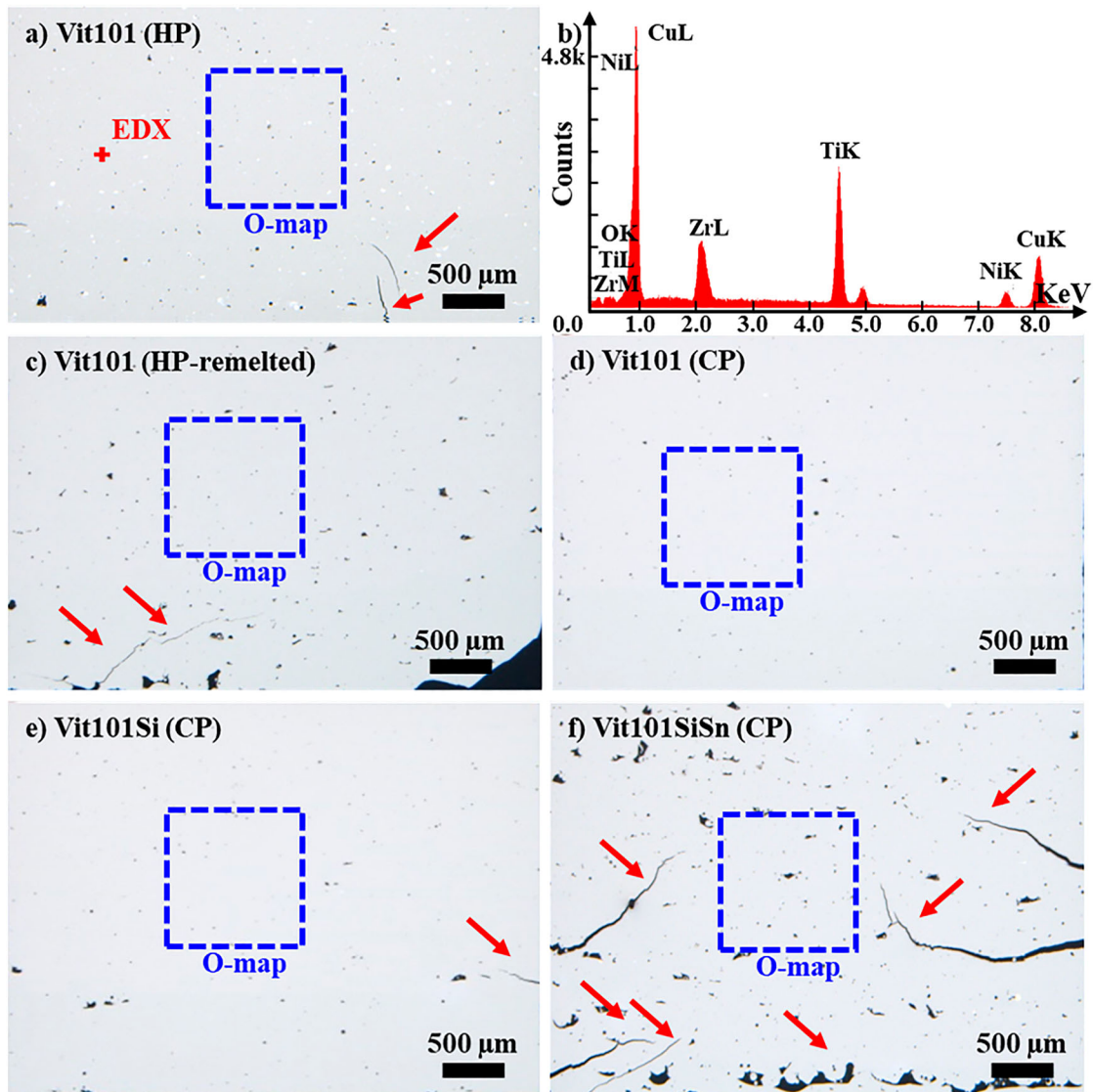
Figure 1. Optical micrographs of additively manufactured samples, showing the cross-section along the build direction of (a) HP Vit101 and its representative; (b) EDX result; (c) HP remelted Vit101; and CPs (d) Vit101; (e) Vit101Si and (f) Vit101SiSn.

compose the base alloy, i.e. Cu, Ti, Zr, Ni and oxygen. To investigate the spatial distribution of oxygen along the build direction, an electron microprobe was used to generate an elemental mapping. The measurement region of each sample is marked in the micrographs depicted in Figure 1 and the results are exhibited in Figure 2.

The distribution of oxygen was found to be homogeneous at the micron scale for all investigated samples, exposed by the featureless micrographs. The lack of elemental segregation supports the notion that a homogeneous, likely amorphous single phase was formed. Quantitative analyses suggest concentrations below 1% in all findings, although accurate EMP measurements of oxygen are challenging due to the high adsorption of low-energy X-rays. Therefore, complementary quantitative studies were carried out with carrier gas hot extraction analysis.

Figure 3 displays the oxygen uptake along the production chain of metallic glasses considering the concentration on the feedstocks for gas-atomisation, powders in the 20–63 μm range, and PBFLB/M samples. The concentration in the HP and CP feedstocks for atomisation was estimated by weighted average according to the oxygen content of the individual elements as provided by the manufacturers. HP elements contained approx. 128 ppm oxygen, whereas the CP feedstock contained around 470 ppm. The measured oxygen concentration in the HP-remelted feedstock, which was melted and solidified inside the atomisation chamber, resulted in 256 ± 151 ppm, twice as much as the HP material.

As expected, the oxygen concentration in the alloys increases with each step along the production chain. It is revealed that the CP feedstock purity most contributes to the final concentration in the additively manufactured samples, representing over 50% of the total oxygen content. In contrast, the highest contribution in HP alloys is inherent from the oxygen in the gas-atomised powder, accounting for more than 60% of
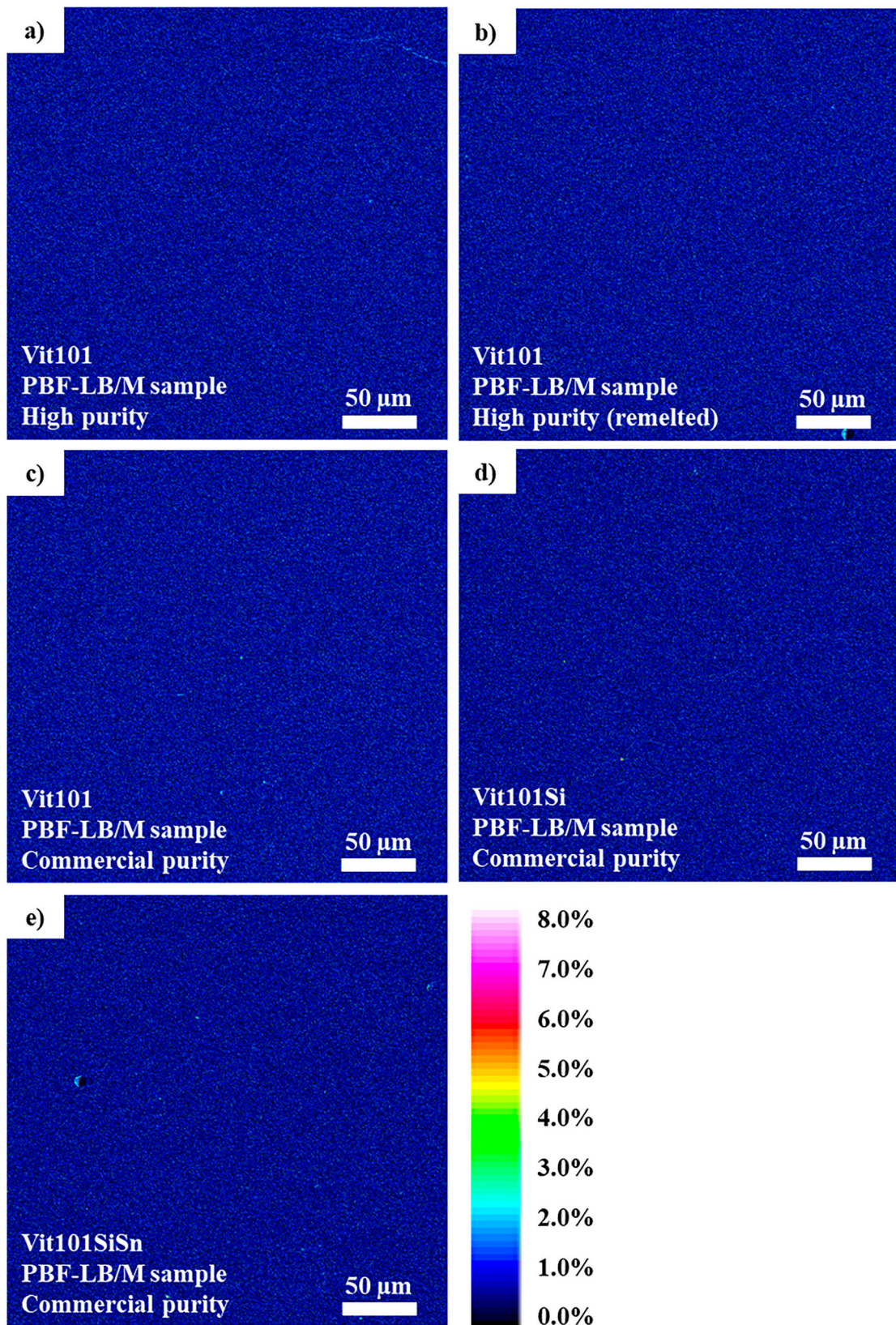
Figure 2. EMP composition elemental mappings of Oxygen for (a) HP Vit101; (b) HP remelted Vit101; and CPs (c) Vit101; (d) Vit101Si and (e) Vit101SiSn. The colour scale bar is attributed to all results.

the overall concentration. A possible explanation might be the higher diffusion gradient between the low-oxygen material and the contaminated atmosphere. According to Stokes–Einstein equation [32], the oxygen diffusion coefficient is inversely proportional to the dynamic viscosity of the solution. Previous experimental research showed the viscosity of some metallic glasses increases with higher oxygen concentrations [33,34]. Consequently, CP materials are presumably more viscous than HP ones. This
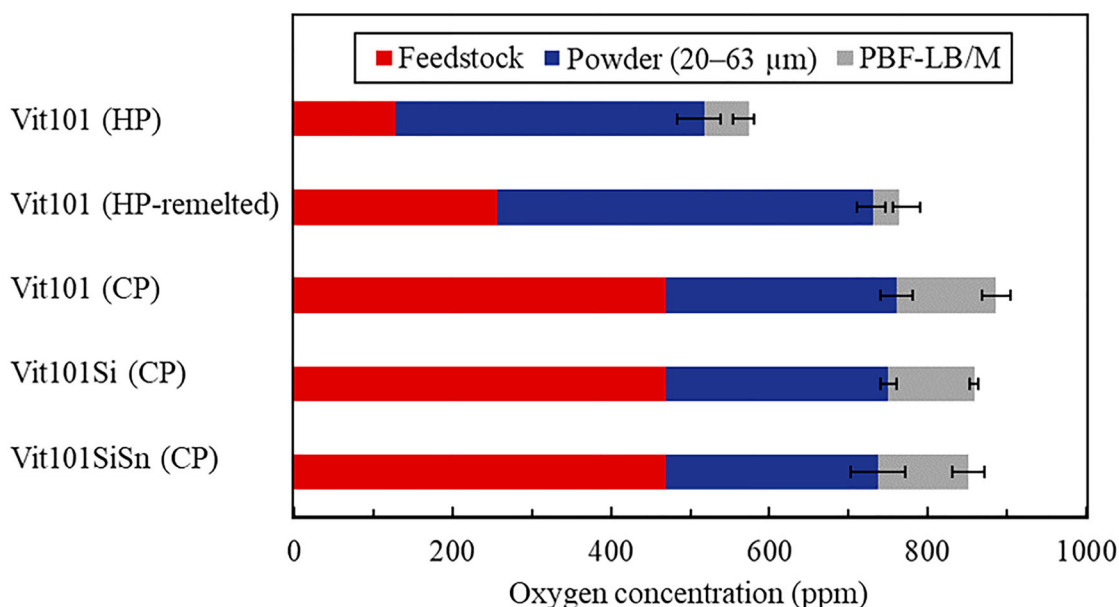
Figure 3. Oxygen uptake along the production chain of Cu–Ti-based metallic glasses via laser powder bed fusion using HP and CP feedstocks.

implies distinct oxygen diffusion gradients, in which the less viscous HP material may be subjected to larger oxygen diffusion.

The uptake during PBF-LB/M processing is inferior to in gas atomisation. A possible explanation might be the closed, circulating gas system of the AM system unit and possibly the better-controlled atmosphere inherent from the comparatively smaller volume chamber [6,10]. Furthermore, the large surface area of powders, mainly responsible for the high oxygen content in droplets [11], is dissolved and remelted into the samples. Consequently, a lower surface area is generated, which accounts for lower oxygen uptake. The presence of oxygen adds up to only ca. 11 ± 4% of final PBF-LB/M samples regardless of the feedstock purity. Overall, using a starting material possessing 75% less oxygen only decreased the final oxygen content in AM samples by about 35%.

Similar oxygen concentrations were measured for Vit101, Vit101Si and Vit101SiSn of CP. The lack of influence of microalloying with Si and Sn on the oxygen uptake is in good agreement with [11].

Considering all feedstock purities, the PBF-LB/M samples presented oxygen levels lower than 900 ppm. At least for Zr-based (AMZ4) BMGs, the GFA is reported to critically sink when the oxygen impurity overcomes 1000 ppm [5,6]. Likewise, the mechanical strength of such Zr alloy strongly worsened for concentrations above 1600 ppm [2], associated with the alloy embrittlement by high oxygen contents [5,6,10]. Studies suggest that the role of oxygen in Cu-based BMGs is as critical as in other Zr- or Ti-based glass formers because most of the oxygen is anyhow introduced by Ti and Zr elements [20]. Hence, determining similar oxygen concentration

limits for Cu–Ti-based metallic glasses is relevant for additive manufacturing production with CP feedstocks.

Besides the impact on mechanical properties, high oxygen levels in BMGs are often associated with a decreased glass-forming ability [5,14–17,20]. Prior research shows that even low concentrations (<0.05%) and variations smaller than 0.01% substantially impact the GFA of a Zr-based alloy [16]. Consequently, the lower thermal stability requires higher cooling rates to bypass crystallisation until vitrification [15,17,18,35]. The oxygen content within the powder is strongly correlated with particle size [2,11,12,14]. As has been previously reported by our group in [11], the fine powder class size < 20 μm contains up to three times more oxygen than particles above 63 μm, due to their significantly larger surface-to-volume ratio. Thus evaluating the glass transition of different class sizes could give a hint of the impact of elevated oxygen contents and cooling rates on the GFA.

Figure 4 shows the heat flow curves obtained via continuous DSC scans of Vit101 and Vit101Si powders with CP. The onsets of glass transition (T_g) and crystallisation event (T_x) are indicated by arrows. The measured oxygen contents in the CP–Vit101 powder class sizes below 20 μm, 20–63 μm, and above 63 μm are 1496 ± 37 ppm, 760 ± 22 ppm and 580 ± 22 ppm, respectively. The corresponding results for the CP–Vit101Si powders are 1505 ± 73 ppm, 750 ± 10 ppm, and 564 ± 16 ppm. Here, the larger surface-to-volume ratio of smaller powder fractions leads to larger oxygen contamination [11].

The glass transition events in the powders of the same alloy occur at equal temperatures regardless of the particle class size. Prior research on HP Vit101
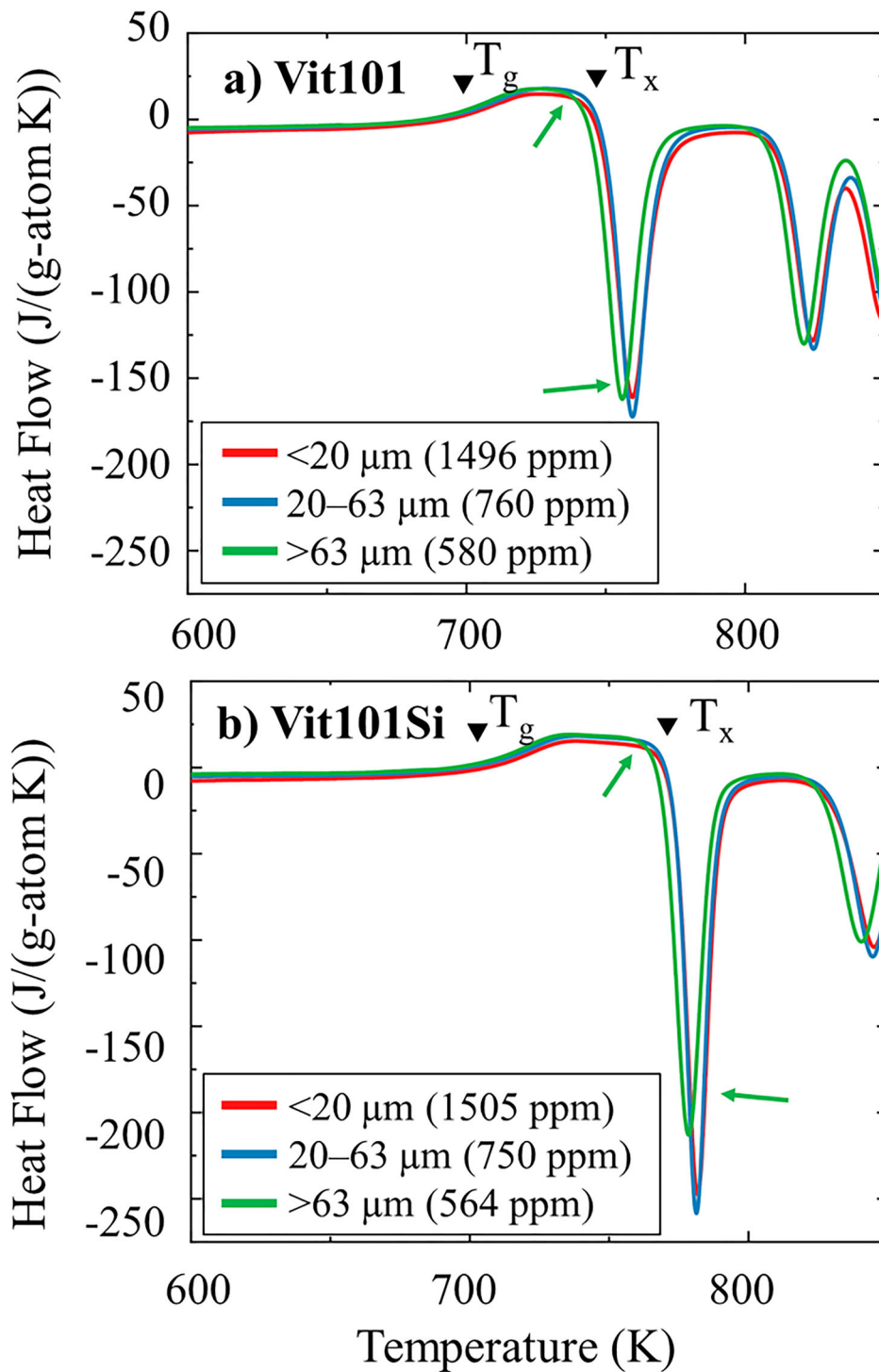
Figure 4. DSC Scans of CP powders of varied class sizes (<20 μm, 23–63 μm, > 63 μm) containing different oxygen concentrations of (a) Vit101 and (b) Vit101Si alloys.

gas-atomised powders in various size ranges reached similar conclusions [12]. The measured onsets of T_g and T_x are 690 and 743 K for Vit101 powders, respectively. Similar findings have been reported in the literature [11,12,24]. Additions of Si to Vit101 enhance the thermal stability of the supercooled liquid against crystallisation, as evidenced by the shift of the onset temperatures T_g to 700 K and T_x to 768 K. The estimated values are consistent with prior research [24,25]. The minor addition of Si is reported to delay the onset of nucleation of a crystalline phase

during molten metal cooling and destabilise oxide nucleation sites, which, in turn, lead to improvements in the GFA [24,25]. The known effect of microalloying on enhancing BMG properties has been extensively reported in the literature [11,20,24,25], often associated with improving the GFA [5,16,24]. Alloys more thermally stable against crystallisation suggest the possible use of CP materials in manufacturing fully amorphous BMGs [5].

For both alloys, the DSC scans of the fractions <20 μm and 20–63 μm evidence the absence of present
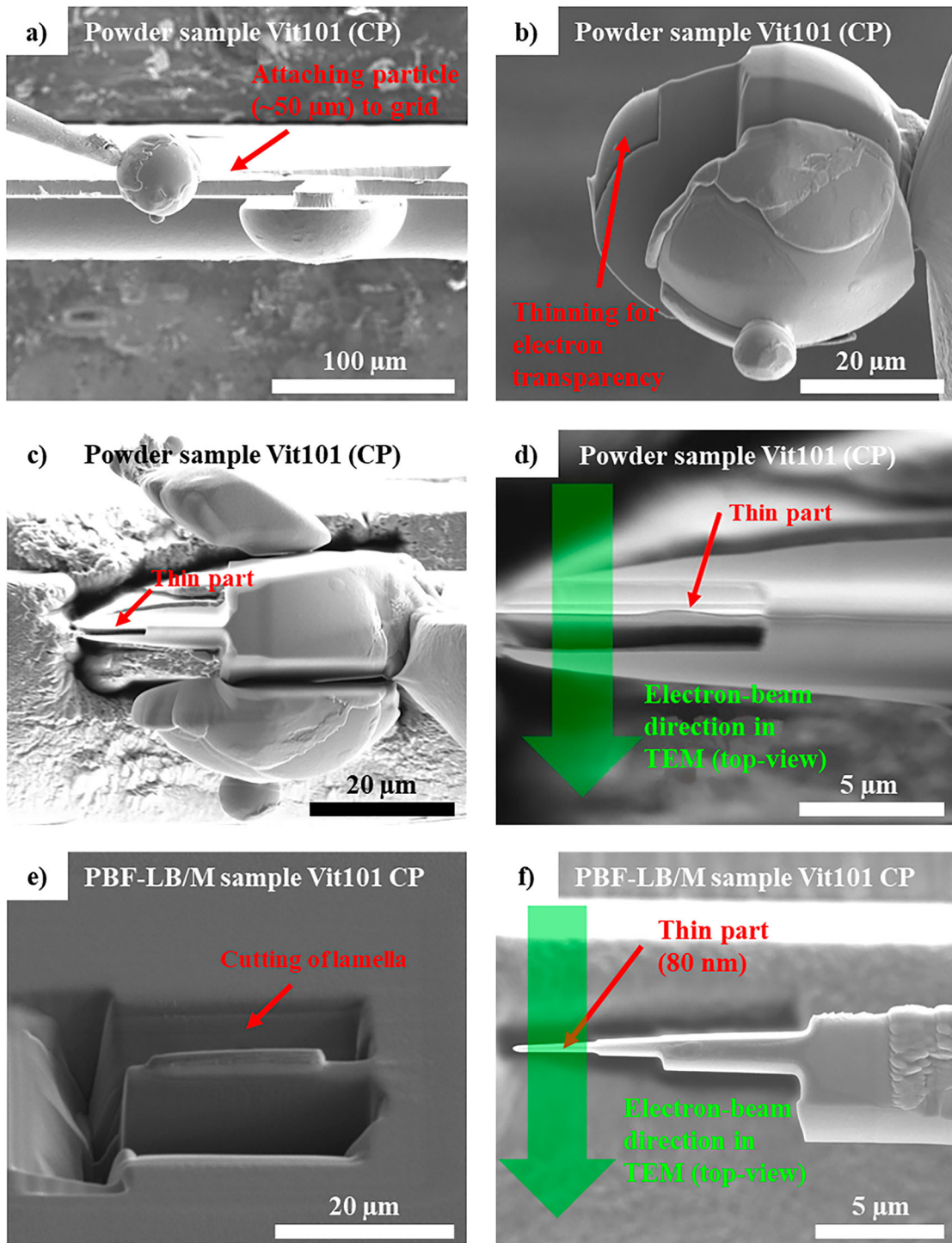
Figure 5. SEM images of the main steps regarding TEM lamella preparation of (a–d) powder and (e–f) PBF-LB/M samples of CP Vit101 alloy.

crystallites. Here, two influence factors for glass formation seem to balance each other: while the smaller particles feature higher oxygen contamination, they also experience faster cooling. Vice versa, the 20–63 μm particles might display a lower oxygen level. Yet, they also exhibit slower cooling rates due to their larger diameter. Higher oxygen levels are often related to the formation of (heterogeneous) oxygen-induced nuclei, which may trigger subsequent crystallisation of the glass phase [4,5,14–18,35]. Hence, the vitrification of the small fraction might benefit from

the cooling that could compensate for the increased oxygen content. On the other hand, Cu–Ti-based metallic glasses might benefit from increased robustness against oxygen, as previously indicated in [36].

Regarding the coarser powder class size (>63 μm), an earlier beginning of the crystallisation event and a slightly lower enthalpy of crystallisation are seen for both Vit101 and Vit101Si, as indicated in the figure with arrows. The causes are most likely explained by the small presence of crystallinity in very large particles as they experience lower cooling rates [11,37].
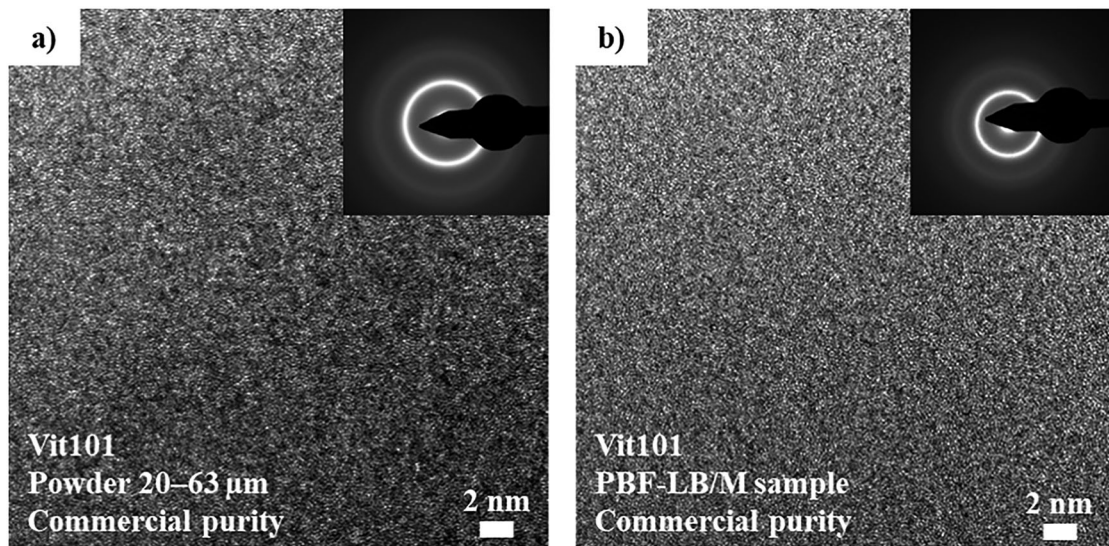
Figure 6. Representative high-resolution TEM of CP Vit101 (a) powder (20–63 μm) and (b) additively-manufactured sample evidence the lack of (nano-)crystallisation and cluster formation, indicating a fully amorphous phase formation.

Previous investigation on the crystallisation behaviour of amorphous as-cast Vit101 alloy revealed a chemical decomposition into copper-enriched and titanium-enriched regions on the nanometre scale [20,38]. The nanocrystals in the amorphous matrix after heat treatment initiated with 2–3 nm in size, recognised with TEM measurements [38].

Since DSC scans and EMP maps are unsuitable for excluding the existence of low fractions of nanocrystallines, powder (20–63 μm) and PBF-LB/M samples of CP Vit101 were evaluated under high-resolution TEM to clarify possible microstructural alterations. Figure 5 displays respective site-specific images of the FIB-lamella preparation and Figure 6 the representative results as observed by HSTEM. Both bright-field micrographs are uniform and featureless, displaying the so-called salt-and-pepper contrast. Likewise, the inserts displaying the selected area diffraction (SAD) pattern show diffuse rings. These results are characteristic of a fully amorphous phase [39]. Thus the presence of oxygen-induced nucleation is rejected, despite the CP feedstock as well as cyclical heating and melting steps characteristics of the PBF-LB/M sample fabrication. As a fully-amorphous phase is reasonably expected in the AM samples with HP, complementary TEM investigation on these samples is waived. Presumably due to the lower affinity of copper to oxygen compared to Zr- and Ti-based alloys [10,11,20,23] and the lower nucleation rate as to some Zr-based alloys [38], CP feedstocks are likely sufficient for processing fully amorphous Cu–Ti–BMGs via PBF-LB/M. Studies have demonstrated that convenient laser settings suffice to provide sufficiently rapid solidification in each layer, so being able to vitrify alloys even with higher oxygen levels [21]. The results are an indication that alloys with low glass-forming ability, inherent for instance either from the alloy composition itself or the high oxygen content from CP starting feedstocks, can be printed into the amorphous state. The findings here presented evidenced the amorphous state of the PBF-LB/M sample with CP, contributing to the economic viability of these alloys at industrial scales.

Taken together, the present research positively contributes to the development of low-cost metallic glass that meets performance requirements for industrial applications, enabling this material class to become more competitive with other alloy types, such as steel or aluminium-based alloys. An oxygen concentration threshold limit to which crystallisation occurs and mechanical properties start to notably deteriorate, as proposed for other glass-forming systems, would be worthwhile to justify CP feedstock use for BMG synthesis via PBF-LB/M of Cu–Ti-based glass-forming alloys. Likewise, experimentally investigating or simulating the oxygen pick-up as a function of specimens' build high and layout is worthwhile. Complex part designs such as in lattice structures [40,41], compliant mechanisms [42,43], or honeycombs [44,45] are extensively subjected to heat dissipation alterations, which may impair the oxygen absorption and cooling and heating rates to a point that crystallisation becomes unavoidable. Hence, a deeper understanding of the crystallisation mechanisms and oxygen uptake during the process chain is essential for upscaling the production of CP metallic glasses via additive manufacturing.

4. Conclusion

This study investigates the effect of oxygen in the production chain of Cu–Ti-based metallic glasses via laser powder bed fusion of metals. The chemical compositions $Cu_{47}Ti_{34}Zr_{11}Ni_8$ (Vit101), $Cu_{47}Ti_{33}Zr_{11}Ni_8Si_1$ (Vit101Si) and $Cu_{47}Ti_{33}Zr_{11}Ni_6Sn_2Si_1$ (Vit101SiSn)

were selected. Feedstocks with CP and HP degrees were gas atomised for powder synthesis, subsequently used for producing additively manufactured samples. It was seen that each processing step contributes to an oxygen level increase in the final PBF-LB/M specimen. The compositions Vit101, Vit101Si and Vit101SiSn contained similar oxygen concentrations, confirming the lack of influence of microalloying additions on oxygen uptake. While the highest contribution in CP materials regards the feedstock itself, the oxygen concentration in HP alloys is inherent mainly from the gas-atomisation process. During PBF-LB/M processability, the oxygen uptake is the lowest. Overall, reducing 75% oxygen in the starting feedstock material only reduced the final oxygen content by about ~35% in the AM samples. The relation between the GFA of powders and oxygen concentration revealed crystallisation events occurring at the same temperature, corroborating an absent influence of oxygen on the thermal stability of the investigated Cu–Ti-based alloys. Observations of CP powder (20–63 μm) and PBF-LB/M samples with high-resolution TEM display typical results of a fully amorphous phase, excluding oxygen-induced nucleation despite higher oxygen levels. The broad implication of the results is that Cu–Ti-based BMGs can be additively manufactured in the amorphous state even with CP feedstocks and the oxygen uptake occurring along the production chain.

Acknowledgements

Disclosure statement

No potential conflict of interest was reported by the author(s).

Funding

Notes on contributors

Erika Soares Barreto is a Research Engineer at the Leibniz-IWT. Her work focuses on powder production via gas atomization and additive manufacturing of glass-forming alloys.

Jan Wegner has a background in Mechanical Engineering and works at the Chair of Manufacturing Technology at the University of Duisburg-Essen, supporting the research on the additive manufacturing of bulk metallic glasses.

Maximilian Frey is a PhD student at the Chair of Metallic Materials at the Saarland University. His research concentrates on the development of bulk metallic glasses.

Stefan Kleszczynski, Dr., is part of the Academic Council of the Chair of Production Engineering and Head of the Rapid Technology Center at the University of Duisburg-Essen.

Ralf Busch, Prof. Dr., is Chair Professor of Metallic Materials at the Saarland University. He works in particular in the field of bulk metallic glasses.

Volker Uhlenwinkel, Dr., is the former Head of the Melt Atomization and Spray Forming group at the Leibniz-IWT. He focused his research on spray compaction, atomization techniques, and powder processability as in additive manufacturing.

Lutz Mädler, Prof. Dr., is the Director of Process Engineering at the Leibniz-IWT and holds a professorship position in Production Engineering at the University of Bremen. His research interests involve, among others, spray processing for particulate materials and nanoparticle technology.

Nils Ellendt, Dr., is Head of Disperse Phase Transition Processes at the Leibniz-IWT and member of the Particles and Process Engineering group at the University of Bremen. The focus of his research is mostly on droplet generation and the scaling to more complex atomization processes.

ORCID

Erika Soares Barreto http://orcid.org/0000-0002-5139-4893

References

[1] Wegner J, Frey M, Kleszczynski S, et al. Influence of process gas during powder bed fusion with laser beam of Zr-based bulk metallic glasses. Procedia CIRP. 2020;94:205–210.

[2] Wegner J, Frey M, Piechotta M, et al. Influence of powder characteristics on the structural and the mechanical properties of additively manufactured Zr-based bulk metallic glass. Mater Des. 2021;209:1–12.

[3] Luo N, Huber F, Ciftci N, et al. Laser powder bed fusion of FeCoBSiNb–Cu bulk metallic glass composites: processing, microstructure and mechanical properties. Mater Sci Eng A. 2022;849. Article No. 143405. DOI:10.1016/j.msea.2022.143405

[4] Sohrabi N, Jhabvala J, Logé RE. Additive manufacturing of bulk metallic glasses—process, challenges and properties. A Rev Metal. 2021;11(8):1279. DOI:10.3390/met11081279.

[5] Liu CT, Chisholm MF, Miller MK. Oxygen impurity and microalloying effect in a Zr-based bulk metallic glass alloy. Intermetallics. 2002;10(11–12):1105–1112.

[6] Deng L, Kosiba K, Limbach R, et al. Plastic deformation of a Zr-based bulk metallic glass fabricated by selective laser melting. J Mater Sci Technol. 2021;60:139–146.

[7] Pacheco V, Karlsson D, Marattukalam JJ, et al. Thermal stability and crystallization of a Zr-based metallic glass produced by suction casting and selective laser melting. J Alloys Compd. 2020;825. Article No. 153995. DOI:10.1016/j.jallcom.2020.153995.

[8] Frey M, Wegner J, Neuber N, et al. Thermoplastic forming of additively manufactured Zr-based bulk metallic glass: a processing route for surface finishing of complex structures. Mater Des. 2021;198:1–8.

[9] Soares Barreto E, Uhlenwinkel V, Frey M, et al. Influence of processing route on the surface reactivity of Cu47Ti33Zr11Ni6Sn2Si1 metallic glass. Metals (Basel). 2021;11(8):1173. DOI:10.3390/met11081173

[10] Madge SV, Greer AL. Laser additive manufacturing of metallic glasses: issues in vitrification and mechanical properties. Oxford Open Mater Sci. 2020;1(1):1–13.

[11] Soares Barreto E, Frey M, Wegner J, et al. Properties of gas-atomized Cu-Ti-based metallic glass powders for additive manufacturing. Mater Des. 2022;215:1–11.

[12] Sordelet DJ, Rozhkova E, Besser MF, et al. Consolidation of gas atomized $Cu_{47}Ti_{34}Zr_{11}Ni_8$ amorphous powders. J Non Cryst Solids. 2003;317(1-2):137–143.

[13] Pauzon C, Dietrich K, Forêt P, et al. Control of residual oxygen of the process atmosphere during laser-powder bed fusion processing of Ti–6Al–4V. Additive Manufact. 2021;38:1–10.

[14] Jonas I, Hembree W, Yang F, et al. Industrial grade versus scientific pure: influence on melt properties. Appl Phys Lett. 2018;112(17):1–4.

[15] Gebert A, Eckert J, Schultz L. Effect of oxygen on phase formation and thermal stability of slowly cooled Zr65Al7.5Cu17.5Ni10 metallic glass. Acta Mater. 1998;46(15):5475–5482.

[16] Kündig AA, Lepori D, Perry AJ, et al. Influence of low oxygen contents and alloy refinement on the glass forming ability of Zr52.5Cu17.9Ni14.6Al10Ti5. Mater Trans. 2002;43(12):3206–3210.

[17] Neto C, Pereira ND, Antonio FS, et al. Phase formation maps in Zr48Cu46.5Al4Nb1.5 bulk metallic glass composites as a function of cooling rate and oxygen concentration. Mater Charact. 2019;158. Article No. 109932. DOI:10.1016/j.matchar.2019.109932

[18] Neto C, Soares ND, Pereira C, et al. Glass forming ability and continuous-cooling-transformation (CCT) diagrams of vitreloy 105 as function of cooling rate and oxygen concentration. J Non Cryst Solids. 2020;528:1–10.

[19] Murty BS, Ping DH, Hono K, et al. Influence of oxygen on the crystallization behavior of Zr65Cu27.5Al7.5 and Zr66.7Cu33.3 metallic glasses. Acta Mater. 2000;48(15):3985–3996.

[20] Park ES, Chang HJ, Kim DH. Improvement of glass-forming ability and phase separation in Cu–Ti-rich Cu–Ti–Zr–Ni–Si bulk metallic glasses. J Alloys Compd. 2010;504:S27–S30.

[21] Bordeenithikasem P, Stolpe M, Elsen A, et al. Glass forming ability, flexural strength, and wear properties of additively manufactured Zr-based bulk metallic glasses produced through laser powder bed fusion. Additive Manufact. 2018;21:312–317.

[22] Marattukalama JJ, Pacheco V, Karlsson D, et al. Development of process parameters for selective laser melting of a Zr-based bulk metallic glass. Additive Manufact. 2020;33:1–8.

[23] Sohrabi N, Schawe JEK, Jhabvala J, et al. Critical crystallization properties of an industrial-grade Zr-based metallic glass used in additive manufacturing. Scr Mater. 2021;199:1–5.

[24] Garrett GR, Demetriou MD, Chen J, et al. Effect of microalloying on the toughness of metallic glasses. Appl Phys Lett. 2012;101(24):1–3.

[25] Choi-Yim H, Busch R, Johnson WL. The effect of silicon on the glass forming ability of the Cu47Ti34Zr11Ni8 bulk metallic glass forming alloy during processing of composites. J Appl Phys. 1998;83(12):7993–7997.

[26] Ciftci N, Ellendt N, Soares Barreto E, et al. Increasing the amorphous yield of {(Fe0.6Co0.4)0.75B0.2Si0.05}96Nb4 powders by hot gas atomization. Adv Powder Technol. 2018;29-(2):380–385.

[27] Shao L, Ketkaew J, Gong P, et al. Effect of chemical composition on the fracture toughness of bulk metallic glasses. Materialia. 2020;12. Article No. 100828. DOI:10.1016/j.mtla.2020.100828

[28] Hofmann DC, Bordeenithikasem P, Pate A, et al. Developing processing parameters and characterizing microstructure and properties of an additively manufactured FeCrMoBC metallic glass forming alloy. Adv Eng Mater. 2018;20(10):1–11.

[29] Pauly S, Schricker C, Scudino S, et al. Processing a glass-forming Zr-based alloy by selective laser melting. Mater Des. 2017;135:133–141.

[30] Chouhan A, Hesselmann M, Toenjes A, et al. Numerical modelling of in-situ alloying of Al and Cu using the laser powder bed fusion process: A study on the effect of energy density and remelting on deposited track homogeneity. Additive Manufact. 2022;59:1–16.

[31] Williams E, Lavery N. Laser processing of bulk metallic glass: A review. J Mater Process Technol. 2017;247:73–91.

[32] Miller CC. The Stokes-Einstein law for diffusion in solution. Proc The Royal Soc A: Mathemat, Phys Eng Sci. 1924;106(740):724–749.

[33] Kübler A, Eckert J, Gebert A, et al. Influence of oxygen on the viscosity of Zr–Al–Cu–Ni metallic glasses in the undercooled liquid region. J Appl Phys. 1998;83(6):3438–3440.

[34] Mizuno A, Harada T, Watanabe M. Effect of minor addition of oxygen on bulk metallic glass formation of binary Cu–Zr alloys via containerless processing. Physica Status Solidi (b). 2020;257(11). DOI:10.1002/pssb.202000140

[35] Lin XH, Johnson WL, Rhim WK. Effect of oxygen impurity on crystallization of an undercooled bulk glass forming Zr–Ti–Cu–Ni–Al alloy. Mater Trans JIM. 1997;38(5):473–477.

[36] Bochtler B. Thermophysical and structural investigations of a CuTi- and a Zr-based bulk metallic glass, the influence of minor additions, and the relation to thermoplastic forming [Dissertation]. University of Saarland; 2019.

[37] Ciftci N, Ellendt N, Coulthard G, et al. Novel cooling rate correlations in molten metal Gas atomization. Metallurg Mater Trans B. 2019;50:666–677.

[38] Glade SC, Löffler JF, Bossuyt S, et al. Crystallization of amorphous $Cu_{47}Ti_{34}Zr_{11}Ni_8$. J Appl Phys. 2001;89-(3):1573–1589.

[39] Suryanarayana C, Inoue A. Metallic Glasses. Ullmann's encyclopedia of industrial chemistry. Weinheim: Wiley-VCH Verlag GmbH; 2012.

[40] Yang C, Zhang C, Xing W, et al. 3D printing of Zr-based bulk metallic glasses with complex geometries and enhanced catalytic properties. Intermetallics. 2018;94:22–28.

[41] Chen SH, Cheng HY, Chan KC, et al. Metallic glass structures for mechanical-energy-dissipation purpose. A Rev Metas. 2018;8(9):1–15.

[42] Homer ER, Harris MB, Zirbel SA, et al. New methods for developing and manufacturing compliant mechanisms utilizing bulk metallic glass. Adv Eng Mater. 2014;16(7):850–856.

[43] Wegner J, Frey M, Busch R, et al. Additive manufacturing of a compliant mechanism using Zr-based bulk metallic glass. Addit Manufact Lett. 2021;1:1–6.

[44] Sarac B, Ketkaew J, Popnoe DO, et al. Honeycomb structures of bulk metallic glasses. Adv Funct Mater. 2012;22(15):3161–3169.

[45] Wegner J, Frey M, Stiglmair P, et al. Mechanical properties of honeycomb structured Zr-based bulk metallic glass specimens fabricated by laser powder Bed fusion. S Afr J Ind Eng. 2019;30(3):32–40.